Interface Debonding Defect of a Concrete-Filled Steel Tube Using PZT Technology

B. Li
College of Civil Engineering, Hunan University, Changsha, 410082, Hunan, China
Department of Civil Engineering, Guangxi University of Technology, Liuzhou, Guangxi, China

B. Xu
College of Civil Engineering, Hunan University, Changsha, 410082, Hunan, China

X. Z. Zhang
KPFF Consulting Engineers, Los Angeles, CA, USA

SUMMARY:
In this paper a novel active interfacial debonding detection method for rectangular Concrete-Filled Steel Tubes (CFSTs) based on the wavelet packet energy spectrum (WPES) of the measurement of Piezoelectric Lead Zirconate Titanate (PZT) patches is proposed firstly and is tested with a scaled rectangular CFST specimen with artificially mimicked debonding defects with different sizes. By embedding PZT based functional smart aggregates (SAs) in concrete core as actuators and pasting PZT patches on the predetermined locations of the outer surfaces of the steel tube of the specimen as sensors, the debonding regions of the CFST specimen are detected. Test results show the WPES of the measurements PZT patches on debonding region has obvious variation. Based on the WPES, a damage index called weighted variation of WPES (WVWPES) is defined and the artificially mimicked debonding regions are detected successfully. Results show that the defined index is sensitive to the debonding defect.

Keywords: Debonding detection, wavelet packet energy spectrum, Concrete-Filled Steel Tubes, PZT

1. INSTRUCTIONS

Concrete-Filled Steel Tubes (CFSTs) have been widely employed in high-rise buildings and bridges as a typical composite member in recent years because of the excellent mechanical performance such as high load-carrying capability, good ductility and energy assumption capability. The quality of concrete pumping and pouring, the change of temperature, the shrinkage and creep of the mass concrete core and so on may induce the interfacial debonding defect between the steel and inner concrete core of CFST. The interfacial debonding defect can weaken the confinement effect of steel tube on the concrete core which induces the decrease in load-carrying capacity and in the ductility of the CFST under earthquake and cyclic loadings. Unfortunately, such debonding damage and the voids cannot be visually identified.

Various traditional Nondestructive Evaluation (NDE) technologies have shown their potential for detecting damage in reinforced concrete, but their suitability and effectiveness for debonding monitoring of CFST is still an open research topic. Li and Han (2000) presented an approach for the detection of debonding between the steel walls and concrete of CFST members by using ultrasonic testing and the results showed the acoustic parameters could reflect the bonding condition between the steel tube and core concrete wall. Moreover, debonding defect detection for CFST by traditional impact echo method heavily depends on the workmanship.

In recent years, piezoelectric-based approach has been widely recognized as one of the most promising active structural health monitoring (SHM) techniques for engineering structures because of advantages of light weight, the availability in different shapes, quick and broadband frequency response, low price, and the ability of being employed as actuators and sensors. Early application of PZT-based

damage detection methodologies is mainly based on impedance analysis and many scholars have carried out study of this subject. Saafi and Sayyah (2001) presented an array of piezoelectric transducers to detect and to localize disbands and debonding of advanced composite reinforcement of concrete structures according to the difference between the current transfer function and baseline transfer function. Wu and Chang (2006a, 2006b) performed an investigation to detect debonding in reinforced concrete (RC) structures utilizing built-in piezoelectric discs as sensors and actuators in a pitch-catch mode and the test results clearly indicate that debonding between concrete and rebar and yielding in rebar can be detected. Song et al. (2008) presented a tutorial and a review on the PZT-based smart aggregates (SAs) as multi-functional sensors for RC structures. Recent studies show the SA can be successfully utilized in the monitoring of typical structure members and structures including RC beams, columns, shear walls and frames under static loading (Bhalla and Soh, 2004, Laskar et al., 2009, and Song et al., 2007, 2009), cyclic reversed loading and seismic loading (Gu et al., 2010, and Moslehy et al., 2010).

This study aims at the development of an active interfacial debonding defect detection approach for CFSTs using the wavelet package energy spectrum (WPES) analysis on the measurement of PZT patches. The performance of the methodology is validated with a test for a CFST specimen with artificially mimicked debonding damages by installing some thin styrofoam plates with different sizes on the inner surfaces of the steel tube before casting the concrete. Results show that the WPES of the measurement from PZT patches is more sensitive to debonding defect.

2. SMART AGGREGATES BASED ON PZT AND CFST TEST SPECIMEN

2.1 Manufacture of Smart aggregates

Piezoelectric material can be utilized as both actuators and patches in structural health monitoring. In the term of monitoring the interfacial condition of CFST members, the PZT actuator should be pre-embedded into the concrete core. In order to protect the brittle piezoelectric transducer from damage, smart aggregates (SAs) which package a PZT patch to be used as an actuator in a small cement mortar block are used. Before being packaged in the cement mortar block, the piezoelectric patch is applied with an insulation coating to protect it from the influence of water and moisture. The employed PZT patch has a dimension of 10mm×10 mm×0.3 mm and then the piezoelectric patch is embedded into a 10mm×10mm×10mm cement mortar block. Figure 2.1 shows an example of the SA with a PZT patch embedded.

Figure 2.1. SA with embedded PZT patch and wire

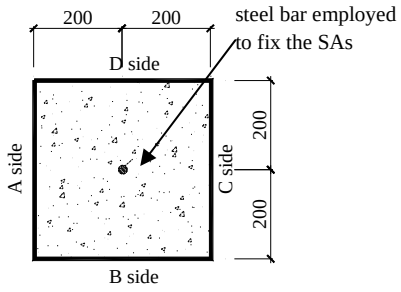

Figure 2.2. Cross section of the CFST specimen

2.2 CFST test specimen

A scale CFST specimen with artificially mimicked debonding defect is designed and constructed in lab. The dimension of the cross section of the rectangular CFST column specimen is 400mm×400mm and the height is 1200mm. The thickness of the steel tube is 2mm. The cross section of the rectangular CFST specimen is shown in Figure 2.2. In order to fix the SAs on designed location before casting concrete, a steel bar is employed and fixed in the center of the column parallel to its vertical axial. The wires of the SAs are fixed on the steel bar and led out along the steel bar. Totally, 3 SAs are employed

in this test and are located in the center of the CFST specimen at height of 400mm(SA-1), 600mm(SA-2) and 800mm(SA-3) from the bottom of the column, respectively. The debonding between the steel tube and the concrete core is simulated by pasting 4 thin styrofoam plates with different sizes on the four internal surfaces of the steel tube. One styrofoam plate is pasted on one of the 4 inner surfaces of the steel tube. The locations of the debonding on each side of the rectangular CFST specimen and the location of PZT patches are shown in Figure 2.3. The thickness of the employed styrofoam plates is 4mm.

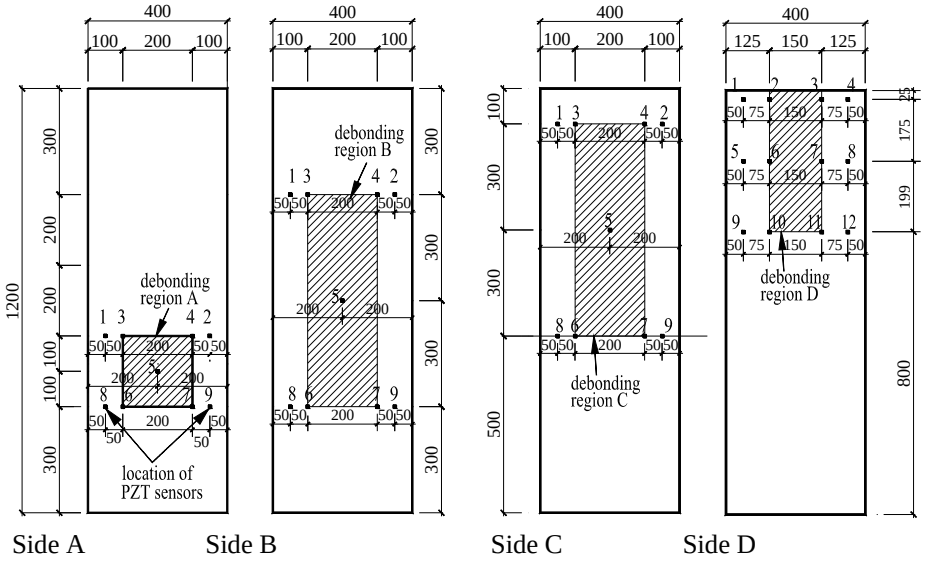

Figure 2.3. Location of debonding regions and PZT patches on the CFST specimen

A total of 48 identical PZT patches are bonded on the four outside surfaces of the rectangular CFST column at designed locations. The arrangement of the PZT patches on the 4 outside surfaces of the rectangular CFST column is shown in Figure 2.3, where some PZT patches are located outside of the artificially mimicked debonding regions and others are within the debonding regions.

3. ACTIVE INTERFACIAL DEBONDING DETECTION APPROACH

In this paper, an evaluation index based on the wavelet packet spectrum on the measurement time history of PZT patches on the steel tube of the CFST structural members induced by the stress wave propagated from the concrete core is proposed and employed to detect the debonding defect between the concrete core and steel tube of the CFST column. The SAs in the concrete core of the CFST column are excited by high frequency signals generated with an arbitrary waveform/function generator and the induced stress wave propagates from concrete core to the steel tube across the interface. Therefore, the outside PZT patches which are employed as sensors are excited by the stress waves and produce charges due to the piezoelectric effect, which are recorded with a high speed data acquisition system. The measurements from the PZT patches are used to detect the debonding. When the stress wave propagates across the interface between the concrete core and the steel tube, it is reflected and scattered at the debonding interface. In this study, the wavelet packet energy spectrum of each PZT patch is determined and employed to detect the debonding defect.

Suppose N_s PZT patches are employed in one surface of the rectangular CFST column. First, the signal output from a PZT patch $k(k=1,\cdots,K)$ is decomposed by *N*-level wavelet packet decomposition into 2^N signal sets as described in the following equation,

$$S_k = s_{k,1} + s_{k,2} + \cdots + s_{k,i} + \cdots + s_{k,2^N-1} + s_{k,2^N} \quad (i = 1,\cdots,2^N \; and \quad k = 1,2,\cdots,K) \tag{3.1}$$

where S_k is original signal, $S_{k,i}$ is signal after N-level wavelet packet decomposition, i is the frequency band index ($i = 1, \cdots, 2^N$), and K is the number of PZT patches employed in each side of the specimen.. $S_{k,i}$ can be expressed as

$$S_{k,i} = \left[s_{k,i,1} \quad s_{k,i,2} \quad \cdots \quad s_{k,i,j} \quad \cdots \quad s_{k,i,m-1} \quad s_{k,i,m} \right], \quad (m = 1, \cdots, M) \tag{3.2}$$

where M is the total number of sampling data of each PZT patch.

The energy vector corresponding to PZT patch k can be defined and expressed as

$$\overline{E_k} = \left[e_{k,1} \quad e_{k,2} \quad \cdots \quad e_{k,i} \quad \cdots \quad e_{k,2^N-1} \quad e_{k,2^N} \right], \quad (k = 1, \cdots, K) \tag{3.3}$$

where $e_{k,i}$ is the corresponding energy of decomposed signal and can be defined as

$$e_{k,i} = \sum_{j=1}^{M} s_{k,i,j}^2 \,, (i = 1, \cdots, 2^N \; and \quad k = 1,2, \cdots, K) \tag{3.4}$$

The WPE of the signals output from PZT patches can be expressed as

$$E_k = \sum_{i=1}^{2^N} e_{k,i} \,, (k = 1, \cdots, K) \tag{3.5}$$

The WPES vector corresponding to PZT patch k can be defined and expressed as

$$ES_k = \left\{ es_{k,1} \quad es_{k,2} \quad \cdots \quad es_{k,i} \quad \cdots \quad es_{k,2^N-1} \quad es_{k,2^N} \right\}, \quad (i = 1, \cdots, 2^N \; and \quad k = 1,2, \cdots, K) \tag{3.6}$$

where $es_{k,i} = e_{k,i} / E_k$. The WPES defined in above Equation describes the wavelet packet energy distribution of the PZT patch k in various frequency bands.

4. TEST RESULT

In this experiment, sweep sinusoidal signal with sweep frequency from 500Hz to 10kHz is used to excite the SAs in the center of the specimen. PZT patches on the four outer surfaces of rectangular CFST column are used as sensors, which signals are recorded in voltage through a high speed data acquisition system with a sampling frequency of 102.4kHz. The WPES of the measurement of each PZT patch on the rectangular CFST specimen is determined according to Equation (2.6).

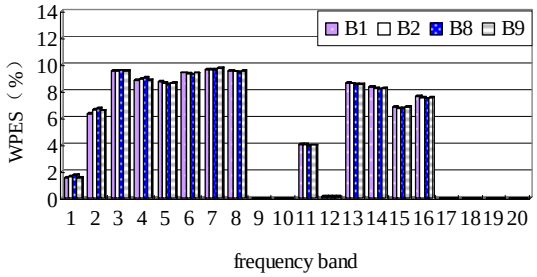

Figure 4.1. WPES of PZT patches on side B with SA-1 as actuator

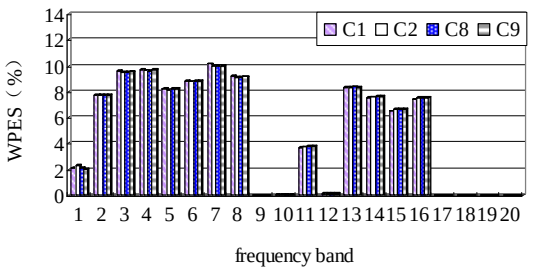

Figure 4.2 WPES of PZT patches on side C with SA-2 as actuator

Here, the WPES of the measurement of three PZT patches located in the bonding regional of Sides B, C are taken as examples and shown in Figures 4.1 and 4.2, respectively. Here, only the WPE values of the first 20th frequency bands after 6-layer wavelet packet decomposition are shown. As shown in the figures, it can be seen clearly that the WPES of the four PZT patches pasted in the bonding region of side B are almost identical. In other words, the WPE of each PZT patch on the bonding region of the same side of the rectangular CFST specimen has very close distribution.

Figures 4.3 and 4.4 show the WPES of the measurements of the PZT patches pasted on the debonding regions on Sides B and C. Different from the PZT patches located in the bonding regions, it is clear the WPES of the PZT patches located in the debonding region shows obvious differences. The WPES of PZT patches located in the debonding region has different characteristics from them of PZT patches within bonding area. This phenomenon means the reflection, refraction and transmission of stress wave across the interface lead to the redistribution of energy within different frequency bands. Therefore, the above findings imply that the interface debonding defect detection can be carried out according to the variation of the WPES of the measurements of the PZT patches.

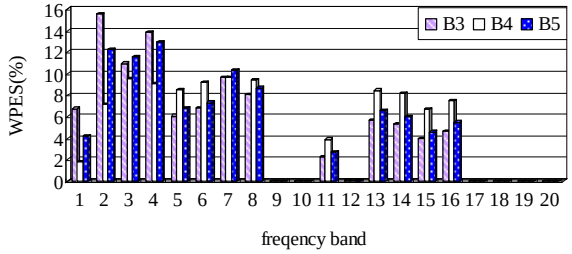

Figure 4.3. WPES of PZT patch on side B with SA-1 as actuator

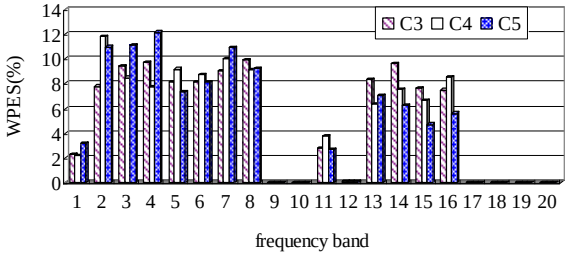

Figure 4.4. WPES of PZT patches on side C with SA-2 as actuator

Based on the above findings, the relative difference of WPES in each frequency band provides an index for the interface condition evaluation and damage detection. The WPES is the distribution of the signal energy in various frequency bands and the sum of the relative change can be defined as a debonding defect evaluation index. An index called as weighted variation of WPES (WVWPES) is defined as follows and employed to evaluate the interface condition of the CFST structural members in the paper,

$$WVWPES_k = \sum_{i=1}^{i=2^N} \left(\left| es_{k,i} - \overline{es}_{k,i} \right| \times \overline{es}_{k,i} \times 100 \right) \tag{4.1}$$

where $es_{k,i}$ is the WPES of the measurement of a PZT patch and $\overline{es}_{k,i}$ is the WPES of the measurement of a PZT patch on bonding region which acts as a weight function. Figure 4.5 shows the WVWEPS values of PZT patches on sides A and C. Here the average of the WPES of the measurement of the PZT patches on bonding region is employed as $\overline{es}_{k,i}$.

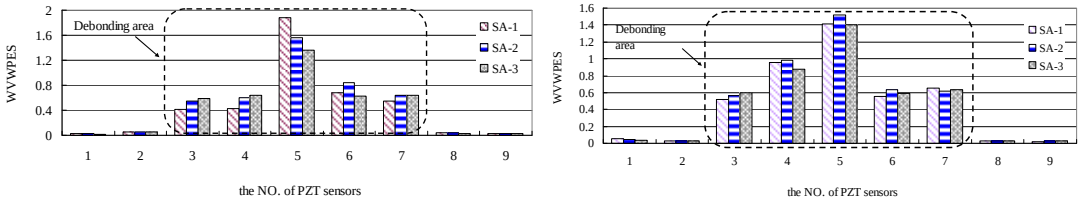

(a) Side A (b) Side C

Figure 4.5. Damage index

From Figure 4.5, it can be seen that the WVWEPS values of the PZT patches on bonding region are obviously smaller than that of PZT patches in debonding region. The interface debonding region can be detected according to the WVWEPS index no matter which SA is employed as the actuator.

5. CONCLUDING REMARKS

An active interfacial debonding defect detection approach based on the wavelet package spectrum analysis on the PZT measurements are proposed. The performance of the proposed approach is validated firstly with a CFST specimen in lab with mimicked debonding defect. Results indicate that the PZT based active interface condition monitoring and evaluation method can be employed in practice for the interfacial debonding detection of CFST columns.

The WPES of signals output from the PZT patches on the bonding region are identical, but the WPES of signals output from the PZT patches on debonding region shows obvious variation. The WPES provides a useful index for the debonding defect detection. A damage index of WVWEPS of the PZT patch on bonding region is much smaller than that of PZT patches on debonding region.

Future research works include the theoretical study on the physical mechanism of the stress wave propagation in concrete and the interface between the concrete and steel tube, and the corresponding numerical simulation.

AKCNOWLEDGEMENT

The authors gratefully acknowledge the support provided by the Program for New Century Excellent Talents in University (NCET-08-0178) and the Fundamental Research Funds for the Central Universities at Hunan University to the second author. The partial support by National Science Foundation (Award No. 0724190) in conducting this research is also greatly appreciated.

REFERENCES

Bhalla, S. and Soh, C.K. (2004). "High frequency piezoelectric signatures for diagnosis of seismic/blast induced structural damage," *NDT & E International*, **37(1)**:23-33

Gu, H., Moslehy, Y., Sanders, D., Song, G., and Mo, Y.L. (2010). "Multi-functional smart aggregate-based structural health monitoring of circular reinforced concrete columns subjected to seismic excitations," *Proceedings of the 12th Biennial International Conference on Engineering, Science, Construction and Operations in Challenging Environments*, ASCE, Honolulu, HI, 2888-2898

Laskar, A., Gu, H., Mo, Y.L., and Song, G. (2009). "Progressive collapse of a 2-story reinforced concrete frame with embedded smart aggregate," Smart Materials and Structures, **18(7)**, 075001

Li, L.Q. and Han, X.J. (2003). "Using ultrasonic method to examine the quality of CFST," *Journal of Nanjing Architectural and Civil Engineering Institute*, **53**, 26-32

Moslehy, Y., Gu, H., Belarbi, A., Mo, Y.L. and Song, G. (2010). "Structural health monitoring of reinforced concrete columns subjected to reversed cyclic loading using innovative smart aggregates," *Proceedings of the 12th Biennial International Conference on Engineering, Science, Construction and Operations in Challenging Environments*, ASCE, Honolulu, HI, 3056-3071

Saafi, M. and Sayyah, T. (2001). "Health monitoring of concrete structures strengthened with advanced composite material using piezoelectric transducers," *Composites*: Part B, **32**:333-342

Song, G., Gu, H., Mo, Y.L., Hsu, T. T. C. and Dhonde, H. (2007). "Concrete structural health monitoring using embedded piezoceramic transducers," *Smart Materials and Structures*, **16(4)**:959-968

Song, G., Gu, H., and Mo, Y.L., (2008). "Smart aggregates: multi-functional sensors for concrete structures-A tutorial and a review," *Smart Materials and Structures*, **17(3)**:033001

Song, G, Yan, S., Sun, W., Gu, H., Huo, L. Sh., Liu, B. and Zhang, Y.G. (2009). "Health monitoring of reinforced concrete shear walls using smart aggregates," *Smart Materials and Structures*, **18**:1-6

Wu, F. and Chang, F.K. (2006a). "Debond detection using embedded piezoelectric elements in reinforced concrete structure –part I: Experiment," *Structural Health Monitoring*, **5(1)**:5-15

Wu, F. and Chang, F.K. (2006b). "Debond detection using embedded piezoelectric elements in reinforced concrete structure –part II: Analysis and Algorithm," *Structural Health Monitoring*, **5(1)**:17-28